An Inverse Kinematic Analysis Modeling on a 6-PSS Compliant Parallel Platform for Optoelectronic Packaging

Fulong Hou, Meizhu Luo, and Zijiao Zhang

***Abstract*—Multiple degree of freedom motion platform is always one of the important components in optoelectronic packaging systems, its characteristics have a vital impact on the performances of optoelectronic packaging. This paper presents a 6-Prismatic-Spherical-Spherical compliant parallel platform for optoelectronic packaging. This platform is a kind of parallel layout structure, which uses the piezoelectric motors as active joints and the large-stroke flexure hinges are employed as passive joints. An inverse kinematic modeling based on elastokinematic analysis is analyzed and deduced. The elastokinematic analysis considers the elastic deformation of the large-stroke flexure hinges in movement process, and improves the positioning accuracy of the compliant parallel platform in applications. The finite element analysis model and the prototype of the compliant parallel platform are developed, and the validity of the proposed method is finally verified. This paper provides a theoretical reference and experimental data for the inverse kinematic analysis of six degrees of freedom motion compliant parallel platforms with large-stroke flexure hinges.**

***Index Terms*—Elastokinematic, inverse kinematic, large-stroke flexure hinge, optoelect-ronic packaging, parallel platform.**

I. Introduction

With the development of optical communication, it is imperative to improve the performances of optoelectronic packaging systems [1]. The six degrees of freedom (6-DOF) motion platforms are a basic component, which has a vital impact on operating characteristics of optoelectronic packaging [2]. To achieve high precision position-orientation adjustment, the 6-DOF motion platforms in optoelectronic packaging systems should have long stroke, high accuracy, high stability, and so on.

Manuscript was submitted for review on 07, January, 2019.

This work was supported in part by the Fundamental Research Funds for the Central Universities of Central South University under Grant 2018zzts470, in part by the National Key Research and Development Program of China under Grant 2017YFB1104800, in part by the National Natural Science Foundation of China under Grant 51575534.

Fulong Hou and Meizhu Luo (Corresponding author) are with the School of Mechanical and Electrical Engineering, Central South University, Changsha, 410083, China (emails: 163712133@csu.edu.cn, luomeizhu2007@126.com).

Zijiao Zhang is with the College of Electrical and Information Engineering, Hunan University, Changsha 410082, China (e-mail: xinruoliuli.07@163.com).

Digital Object Identifier 10.30941/CESTEMS.2019.00011

Compared with the conventional serial platforms, the parallel platforms have the merits of high-stiffness, high bearing capacity, and high-accuracy. The flexure hinges can realize the expected motion through the elastic deformation, the backlash and friction can be avoided compared with conventional mechanism joints [3-5]. Meanwhile, to achieve the adjustment within a large range of travel, the large-stroke flexure hinges are introduced [6, 7]. Therefore, the compliant parallel platforms with large-stroke flexure hinges have both of the great features of the parallel platforms and the flexure hinges, and a long stroke motion can also be achieved. However, the large elastic deformation and the displacement of the rotation center will occur with the large-stroke flexure hinges, it is very hard to obtaining an appropriate kinematic model [8].

In previous studies, many scholars have adopted the pseudo-rigid-body model concept to obtained a more accurate kinematic model of the compliant mechanisms. The elastic deformation of the large-stroke flexure hinges is considered as a rotational motion around a fixed axis, the position of the rotation axis can be determined by experiments or simulations. But for a flexible body in space, the method can not accurately achieve the virtual rotation axis [9, 10]. Some researchers have tried to change the structure of the flexure hinges, limit the offset of the rotating axis on the premise of the large deformation in the flexible hinges, and improve the positioning accuracy of the end platform. But these are limited to special flexible hinges, not suitable for all types [11, 12]. Dong *et. al.* established an inverse kinematics model of a 6-Prismatic-Spherical-Spherical (6-PSS) platform with large-stroke flexure hinges based on finite element analysis (FEA) method. Both flexure hinges and rigid rods are treated as spatial beam structure, the stiffness matrix of the flexible elements are deduced, and the geometric nonlinearity caused by the constant change of the stiffness matrix is solved. However, the calculations are complex and require a lot of iterations [6]. Wang *et. al.* derived the inverse kinematics model of a 6-PSS compliant parallel platform in nonlinear closed-form, and simplified the mathematical complexity while solving the accuracy problem, their works provided more parametric design insights for this type of structure [13]. Shi derived the kinematic model and calibrated the motion of a hexapod platform nano-posioner. They measured the position and posture of the end platform via external measuring equipment, and recalibrated the kinematics model based on the measured experimental data. However, the measurement system is complex and costly [14]. Rouhani *et. al.* developed a method for a microhexapod platform on the basis of the elastokinematic analysis, which considered the change of the rotation center of the flexible hinges in the elastic deformation [15].

In this paper, we develop an elastokinematic analysis based inverse kinematics solution of a 6-PSS compliant parallel platform for optoelectronic packaging. The rest of this paper is organized as follows, the structure design of the 6-PSS compliant parallel platform is introduced in Section II. In section III, the inverse kinematics solution based on elastokinematic analysis is developed. In section IV, the proposed method is verified based on FEA method. In section V, the experimental tests are shown. Finally, the conclusion is given in Section VI.

II. System Description

As shown in Fig. 1, the 6-PSS compliant parallel platform consists of the moving platform, the kinematic limbs, the driving units, and the fixed platform. Each kinematic limb connect the moving platform with the fixed platform by the large-stroke flexure hinges. To achieve a larger travel, the large-stroke flexure hinges are employed as passive joint. They are considered as a slender and spatial beam structure, which can rotate around three axes. The driving units as active joints are fitted on the fixed platform, the piezoelectric motors are employed as actuators for their advantages of high-accuracy, large driving force, small size, and so on. For the chosen materials, it is hoped that the deformation of the flexure hinges in the functional direction will be as large as possible, so the beryllium bronze is selected as the material of the large-stroke flexure hinges. The duralumin is chosen as the material for other parts.

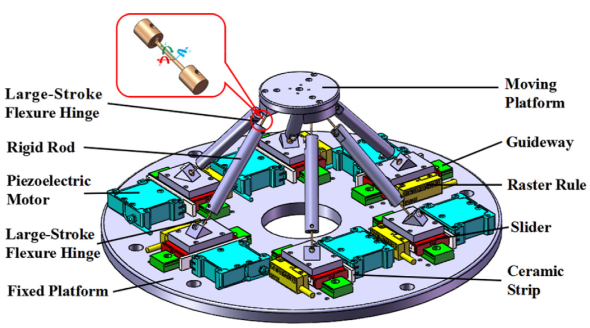

Fig. 1. Basic configuration of the 6-PSS compliant parallel platform.

Fig. 2 shows a picture of the structure about the platform in detail. A reference coordinate system *B-xyz* is fixed to the center point *B* of the fixed platform. A local coordinate system *P-xyz* is attached to the center point *P* of the moving platform. The *z*-axis is perpendicular to the platform and upward, the *x*-axis runs along the angular bisector of the driving units 1 and 6, and the *y*-axis can be given by the right hand rule. The motion direction of the driving units 1, 3, 4, and 6 are along *x*-axis, and the driving units 2 and 5 are along *y*-axis. The main geometric and structure parameters are listed in Table I.

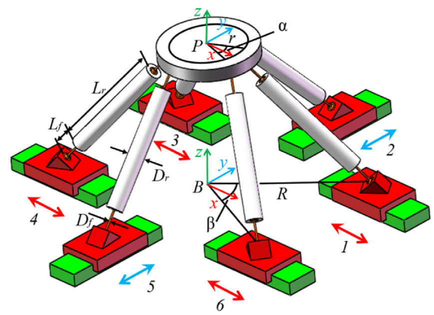

Fig. 2. The structural description about the platform in detail.

TABLE I
THE GEOMETRIC AND STRUCTURE PARAMETERS OF THE 6-PSS COMPLIANT PARALLEL PLATFORM

Item	Value
Diameter of the moving platform r	50 mm
Diameter of the fixed platform R	180 mm
Distribution angle of the upper flexure hinge α	30°
Distribution angle of the lower flexure hinge β	60°
Length of the rigid rod L_r	74 mm
Length of the large-stroke flexure hinge L_f	13 mm
Diameter of the rigid rod D_r	10 mm
Diameter of the large-stroke flexure hinge D_f	1 mm
Density of the rigid rod ρ_r	2700 Kg/m^3
Density of the large-stroke flexure hinge ρ_f	8100 Kg/m^3
Modulus of elasticity of the rigid rod E_r	70 Gpa
Modulus of elasticity of the large-stroke flexure hinge E_f	130 Gpa

III. Inverse Kinematic Modeling

In this section, an elastokinematic analysis based inverse kinematics solution of a 6-PSS compliant parallel platform is developed. Each kinematic limb consists of the large-stroke flexure hinges at both ends and a rigid rod in the middle, and they are all considered as flexible body. The moving platform can be treated as rigid body. It should be noted that the six driving units can be regarded as special flexible body, they have only one degree of freedom as a variable defined by the input values.

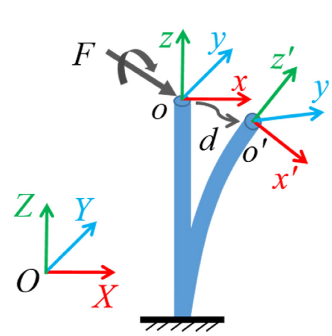

Fig. 3. A flexible body in space.

Fig. 3 shows a picture of a flexible body in space. Within the elastic limit range, the loads are applied on a certain point for flexible body in space, then the flexibility model can be established in the local coordinate system as follows:

$$d = C \cdot F \tag{1}$$

where d is defined as the nodal displacements, F is defined as the nodal loads, and C is the flexibility matrix of the flexible body. Specifically, C can be obtained as follows [16]:

$$C = \begin{bmatrix} \frac{4l^3}{3\pi Er^4} & 0 & 0 & 0 & \frac{2l^2}{\pi Er^4} & 0 \\ 0 & \frac{4l^3}{3\pi Er^4} & 0 & -\frac{2l^2}{\pi Er^4} & 0 & 0 \\ 0 & 0 & \frac{l}{\pi Er^2} & 0 & 0 & 0 \\ 0 & -\frac{2l^2}{\pi Er^4} & 0 & \frac{4l}{\pi Er^4} & 0 & 0 \\ \frac{2l^2}{\pi Er^4} & 0 & 0 & 0 & \frac{4l}{\pi Er^4} & 0 \\ 0 & 0 & 0 & 0 & 0 & \frac{2l}{\pi Gr^4} \end{bmatrix} \tag{2}$$

where E, G, l, and r represent the Young's modulus of the materials, the Shear modulus of the materials, the length, and the radius of cross section for the flexible body.

The description of the coordinate systems for i^{th} (i = 1, 2, . . . , 6) kinematics chain as shown in Fig. 4. The connection point between the moving platform and i^{th} upper flexure hinge is defined as P_i, a local coordinate system P_i-xyz is fixed to the point P_i, which always parallel to P-xyz frame. The other three local coordinate systems are fixed at the bottom of the upper flexure hinge denoted by u_i-xyz, the rigid rod denoted by r_i-xyz, and the lower flexure hinge denoted by l_i-xyz separately. The z axis point from bottom to top along the geometric axis. A local coordinate frame s_i-xyz is attached to the center of gravity at driving units, the z axis along the only moving direction of the driving units.

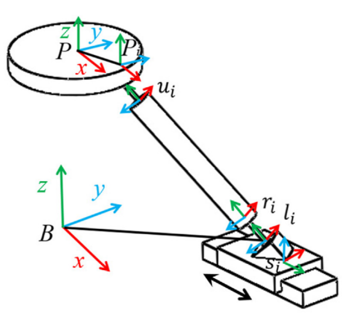

Fig. 4. The description of the coordinate systems for i^{th} kinematics chain

For the i^{th} kinematics chain, referring to Eqs. (1), the flexibility models in the local coordinate system for above flexible bodies can be derived as follows:

$$d_{u_i} = {}^{u_i}C_u \cdot F_{u_i} \tag{3}$$

$$d_{r_i} = {}^{r_i}C_r \cdot F_{r_i} \tag{4}$$

$$d_{l_i} = {}^{l_i}C_l \cdot F_{l_i} \tag{5}$$

$$d_{s_i} = {}^{s_i}C_s \cdot F_{s_i} \tag{6}$$

where ${}^{u_i}C_u$, ${}^{r_i}C_r$, ${}^{l_i}C_l$, and ${}^{s_i}C_s$ represent the flexibility matrix of the upper flexure hinge, the rigid rod, the lower flexure hinge, and the driving units in the local coordinate frame. The flexibility matrixs are considered to be invariant matrices based on linear assumption. Note that ${}^{s_i}C_s$ as a flexibility matrix, in which a large value is given to the parameter associated with the input displacement, and the other parameters are zero.

Further, d_{u_i}, d_{r_i}, d_{l_i}, and d_{s_i} can be converted to the displacement at the point P_i of the i^{th} kinematics chain in the coordinate system P_i-xyz respectively, as follows:

$$d^u_{P_i} = {}^{P_i}_{u_i}J \cdot d_{u_i} \tag{7}$$

$$d^r_{P_i} = {}^{P_i}_{r_i}J \cdot d_{r_i} \tag{8}$$

$$d^l_{P_i} = {}^{P_i}_{l_i}J \cdot d_{l_i} \tag{9}$$

$$d^s_{P_i} = {}^{P_i}_{s_i}J \cdot d_{s_i} \tag{10}$$

where $d^u_{P_i}$, $d^r_{P_i}$, $d^l_{P_i}$, and $d^s_{P_i}$ represent the displacement in the local coordinate system P_i-xyz at the point P_i that are triggered by the displacements of the upper flexure hinge, the rigid rod, the lower flexure hinge, and the driving units. ${}^{P_i}_{u_i}J$, ${}^{P_i}_{r_i}J$, ${}^{P_i}_{l_i}J$, and ${}^{P_i}_{s_i}J$ are defined as the transformation matrix from u_i-xyz, r_i-xyz, l_i-xyz, and s_i-xyz frame to P_i-xyz frame.

Let J be the equivalent transformation matrix from the frame m to n, and which can be derived as follows [17]:

$${}^n_mJ = \begin{bmatrix} {}^n_mR_{3\times3} & -{}^n_mR_{3\times3} \cdot {}^n_mT_{3\times3} \\ O_{3\times3} & {}^n_mR_{3\times3} \end{bmatrix} \tag{11}$$

where $O_{3\times3}$ is the zero matrix. ${}^n_mR_{3\times3}$ and ${}^n_mT_{3\times3}$ denote the rotation matrix and the relative position transformation matrix of the frame m with respect to n, and ${}^n_mT_{3\times3}$ is defined as follows:

$${}^n_mT_{3\times3} = \begin{bmatrix} 0 & -{}^n_mz & {}^n_my \\ {}^n_mz & 0 & -{}^n_mx \\ -{}^n_my & {}^n_mx & 0 \end{bmatrix} \tag{12}$$

Then the displacement of the point P_i in the coordinate frame P_i-xyz can be derived as a linear combination of $d^u_{P_i}$, $d^r_{P_i}$, $d^l_{P_i}$, and $d^s_{P_i}$:

$$d_{P_i} = d^u_{P_i} + d^r_{P_i} + d^l_{P_i} + d^s_{P_i} \tag{13}$$

Let $d_p = \left[x\ y\ z\ \theta_x\ \theta_y\ \theta_z\right]^T$ as the displacement of the moving platform at the center point in the coordinate system P-xyz. The displacement of the point P_i in the coordinate frame P_i-xyz can be represented as follows:

$$d_{P_i} = {}^{P_i}_{P}J \cdot d_P \tag{14}$$

where ${}^{P_i}_{P}J$ represents the transformation matrix from P-xyz coordinate frame to P_i-xyz coordinate frame.

When the moving platform bears a certain loads in the local coordinate system P-xyz, the loads will be distributed to each kinematics chain. For the i^{th} kinematics chain in P_i-xyz frame, the loads can be converted into F_{P_i} at the point P_i. Similarly, he loads are applied to the upper flexure hinge denoted by F_{u_i}, the rigid rod denoted by F_{r_i}, the lower flexure hinge denoted by F_{l_i}, and the driving units denoted by F_{s_i} in the local coordinate system. They can be given as below:

$$F_{u_i} = {}^{u_i}_{P_i}J \cdot F_{P_i} \tag{15}$$

$$F_{r_i} = {}^{r_i}_{P_i}J \cdot F_{P_i} \tag{16}$$

$$F_{l_i} = {}^{l_i}_{P_i}J \cdot F_{P_i} \tag{17}$$

$$F_{s_i} = {}^{s_i}_{P_i}J \cdot F_{P_i} \tag{18}$$

Substituting Eqs. (15)-(18) into Eqs. (3)-(6), and then in Eq. (13) yields:

$$d_{P_i} = ({}^{P_i}_{u_i}J \cdot {}^{u_i}C_u \cdot {}^{u_i}_{P_i}J + {}^{P_i}_{r_i}J \cdot {}^{r_i}C_r \cdot {}^{r_i}_{P_i}J + {}^{P_i}_{l_i}J \cdot {}^{l_i}C_l \cdot {}^{l_i}_{P_i}J + {}^{P_i}_{s_i}J \cdot {}^{s_i}C_s \cdot {}^{s_i}_{P_i}J) \cdot F_{P_i} \tag{19}$$

Therefore, the above equation can be written into:

$$F_{P_i} = ({}^{P_i}_{u_i}J \cdot {}^{u_i}C_u \cdot {}^{u_i}_{P_i}J + {}^{P_i}_{r_i}J \cdot {}^{r_i}C_r \cdot {}^{r_i}_{P_i}J + {}^{P_i}_{l_i}J \cdot {}^{l_i}C_l \cdot {}^{l_i}_{P_i}J + {}^{P_i}_{s_i}J \cdot {}^{s_i}C_s \cdot {}^{s_i}_{P_i}J)^{-1} \cdot d_{P_i} \tag{20}$$

For simplicity, we defined K_i as follows:

$$K_i = ({}^{P_i}_{u_i}J \cdot {}^{u_i}C_u \cdot {}^{u_i}_{P_i}J + {}^{P_i}_{r_i}J \cdot {}^{r_i}C_r \cdot {}^{r_i}_{P_i}J + {}^{P_i}_{l_i}J \cdot {}^{l_i}C_l \cdot {}^{l_i}_{P_i}J + {}^{P_i}_{s_i}J \cdot {}^{s_i}C_s \cdot {}^{s_i}_{P_i}J)^{-1} \tag{21}$$

Substituting F_{P_i} from Eq. (20) and Eq. (21) into Eq. (18) yields:

$$F_{s_i} = {}^{s_i}_{P_i}J \cdot K_i \cdot d_{P_i} \tag{22}$$

Combining (6) and (22), we can get the following equation:

$$d_{s_i} = {}^{s_i}C_s \cdot {}^{s_i}_{P_i}J \cdot K_i \cdot d_{P_i} \tag{23}$$

Using (14) and the above equation, calculating d_{s_i} results in:

$$d_{s_i} = ({}^{s_i}C_s \cdot {}^{s_i}_{P_i}J \cdot K_i \cdot {}^{P_i}_{P}J) \cdot d_P \tag{24}$$

Therefore, when the output displacement d_P of the moving platform at the center point is known, the linear input displacement d_{s_i} of a 6-PSS compliant parallel platform can be given by solving Eq. (24).

IV. Simulations

To investigate the effectiveness of the elastokinematic model about the 6-PSS compliant parallel platform designed. An inverse kinematic solution program by means of MATLAB is developed based on above analysis and deduction. The FEA is carried out by utilizing ANSYS Workbench. Fig. 5 show a simplified FEM model of the 6-PSS compliant parallel platform for simulation.

A. Inverse kinematic analysis

It was assumed that the moving platform has a desired output ($x\ y\ z\ \theta_x\ \theta_y\ \theta_z$). Then the input displacements of the driving units ($d_{s_1}\ d_{s_2}\ d_{s_3}\ d_{s_4}\ d_{s_5}\ d_{s_6}$) will be calculated via inverse kinematic analysis by the elastokinematic model and the FEA model respectively. The inverse kinematics solution results are shown in Table II. It can be found that the errors of the input displacements between the two kinds of inverse solution models are under 0.2μm.

B. Forward kinematic analysis

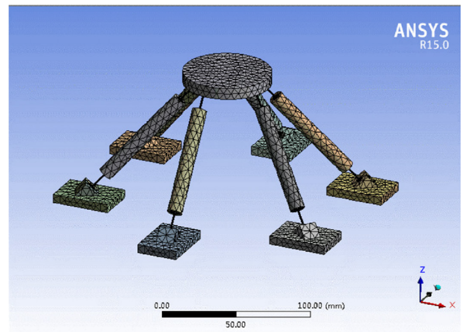

Fig. 5. A FEA model developed in ANSYS Workbench.

TABLE II
THE INVERSE KINEMATICS SOLUTION RESULTS

Output		(6 mm, 0 mm, 0 mm, 0 °, 0 °, 0 °)
Input	Elastokinematic model	(5.9999 mm, 0.5819 mm, 6 mm, 6 mm, -0.5819 mm, 5.9999 mm)
	FEA model	(6 mm, 0.58211 mm, 6 mm, 6 mm, -0.58211 mm, 6 mm)
Output		(0 mm, 6 mm, 0 mm, 0 °, 0 °, 0 °)
Input	Elastokinematic model	(4.2856 mm, 5.9999 mm, -2.7290 mm, 2.7290 mm, 5.9999 mm, -4.2856 mm)
	FEA model	(4.2858 mm, 6 mm, -2.7288 mm, 2.7288 mm, 6 mm, -4.2858 mm)
Output		(0 mm, 0 mm, 6 mm, 0 °, 0 °, 0 °)
Input	Elastokinematic model	(-8.1883 mm, -6.6944 mm, 7.3200 mm, 7.3200 mm, 6.6944 mm, -8.1883 mm)
	FEA model	(-8.1884 mm, -6.6944 mm, 7.3199 mm, 7.3199 mm, 6.6945 mm, -8.1884 mm)
Output		(3 mm, 3 mm, 3 mm, 0 °, 0 °, 0 °)
Input	Elastokinematic model	(1.0486 mm, -0.0563 mm, 5.2955 mm, 8.0245 mm, 6.0563 mm, -3.2369 mm)
	FEA model	(1.0487 mm, -0.0561 mm, 5.2956 mm, 8.0243 mm, 6.0562 mm, -3.2371 mm)
Output		(0 mm, 0 mm, 0 mm, 3 °, 3 °, 3 °)
Input	Elastokinematic model	(1.6990 mm, -1.8456 mm, 1.1017 mm, 0.2602 mm, -1.0025 mm, 0.8555 mm)
	FEA model	(1.6992 mm, -1.8455 mm, 1.1018 mm, 0.26027 mm, -1.0027 mm, 0.85546 mm)

Let the moving platform moved about 6 mm in the x and y direction respectively, and no movement in other directions. And the input displacements of the driving units were given by the FEA model and the elastokinematic model. Then the values were employed to the forward kinematic model by FEA respectively. Fig. 6 shows a picture of the simulation displacements of the platform when x=6mm. By comparing the displacements of the moving platform, the simulation displacements of the center point are about 5.9957mm based on the FEA model and 5.9954mm based on the elastokinematic model. The error between two models are 0.3μm. Similarly, Fig. 7 shows a picture of the simulation displacements of the platform when y=6mm. By comparing the displacements of the moving platform, the simulation displacements of the center point are about 5.991mm based on the FEA model and 5.9906mm based on the elastokinematic model. The error between two models are 0.4μm.

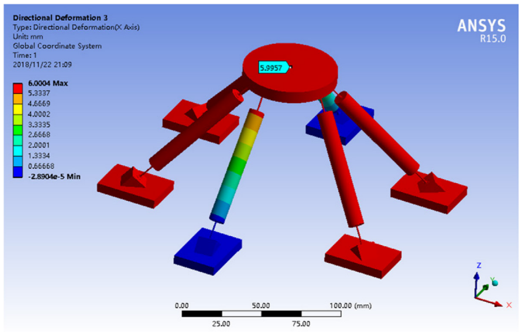

Fig. 6 (a). The simulation displacements of the platform based on the FEA model when x=6mm.

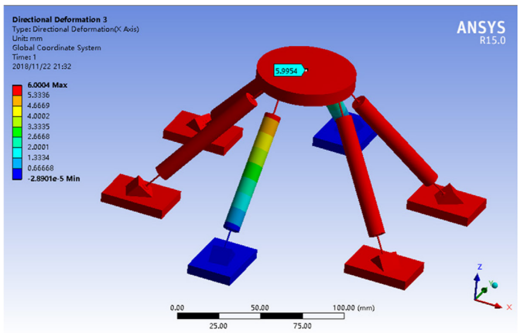

Fig. 6 (b). The simulation displacements of the platform based on the elastokinematic model when x=6mm.

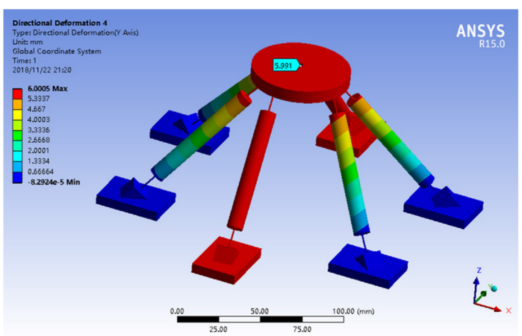

Fig. 7 (a). The simulation displacements of the platform based on the FEA model when y=6mm.

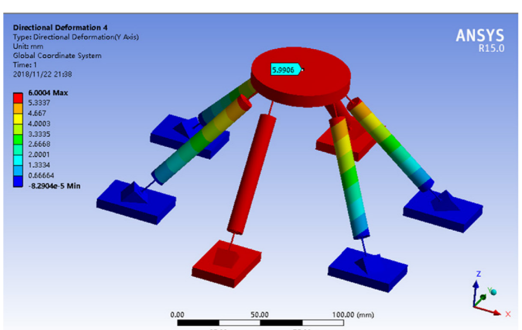

Fig. 7 (b). The simulation displacements of the platform based on the elastokinematic model when y=6mm.

Let the moving platform followed a circular track with a radius of 6mm on the xy plane, and no movement in other directions. And the input displacements of the driving units were given by the FEA model and the elastokinematic model. Then they were employed to the forward kinematic model by FEA respectively. The movement tracks of the moving platform at the center point are shown in Fig. 8. And Fig. 9 shows the track errors of the moving platform on the x and y axes. By comparison, the trajectories obtained by the two models are better fitted with desired trajectory. But due to the coupling of the parallel platforms, the errors will increase relative to uniaxial motion. The maximum track errors of the elastokinematic model in the x direction and y direction are about 4.6μm and 9.5μm, and the maximum track errors of FEA model in the x direction and y direction are about 4.4μm and 9μm. The results analysis show that the errors between the two models are very small.

V. EXPERIMENTS

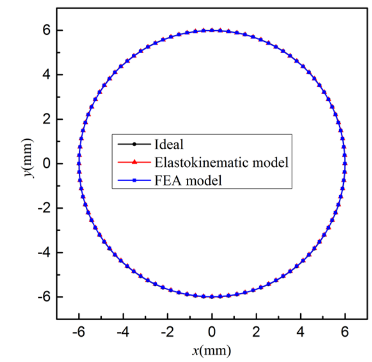

Fig. 8. The movement tracks at the center point of the moving platform.

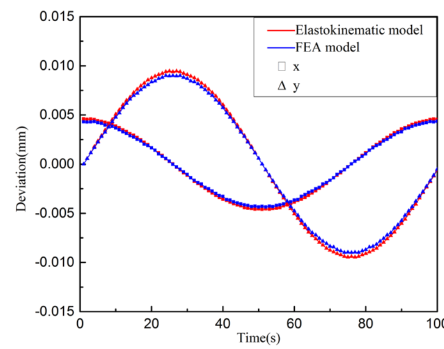

Fig. 9. The track errors in the x and y direction

To further validate the developed method, the prototype of a 6-PSS compliant parallel platform was manufactured as shown in Fig. 10, and an experimental test system based on the 6-PSS compliant parallel platform was also developed as shown in Fig. 11. The platform is controlled in the half-closed loop, and the specific system control diagram is shown in Fig. 12. The movement tracks of the moving platform are measured by means of the laser interferometer (Renishaw XL80, RENISHAW, Inc.). Its maximum sampling frequency can reach 50KHZ, the resolution is about 1nm, and the precision can reach to ±0.5 ppm. Considering that the rotation angle in space is difficult to measure, and the laser interferometer can only measure one-dimensional motion, so only some position points are selected for measurement.

When the moving platform was driven to move about 1 and 6 mm in the x direction, respectively. The input displacements of the driving units were given by the elastokinematic model,

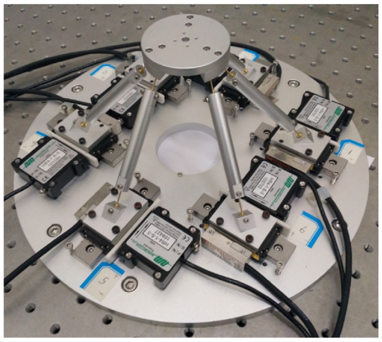

Fig. 10. The prototype of the 6-PSS compliant parallel platform.

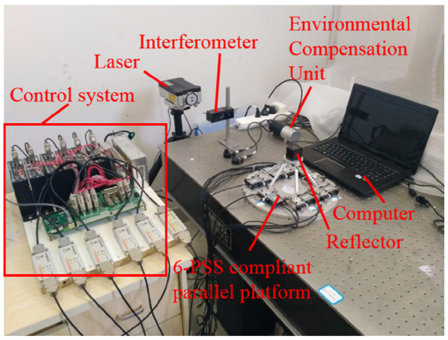

Fig. 11. The experimental test system.

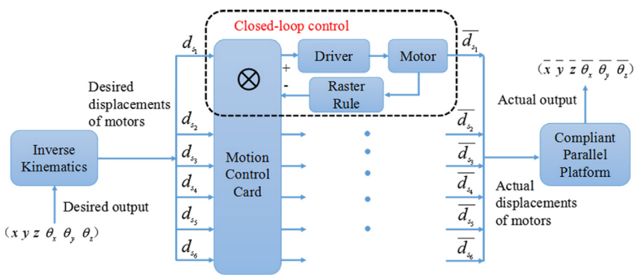

Fig. 12. The system control diagram of the 6-PSS compliant parallel platform.

and then the values were employed to the experimental prototype. Fig. 13 shows a picture of the actual displacement of the moving platform when x=1mm, the experimental results show that the actual displacement is 0.998437mm, the error is 1.563 μm. Fig. 14 shows a picture of the actual displacement of the moving platform when x=6mm, the experimental results show that the actual displacement is 6.019799mm, the error is 19.799 μm.

When the moving platform was driven to move about 1 and 6 mm in the y direction, respectively. The input displacements of the driving units were given by the elastokinematic model, and then the values were employed to the experimental prototype. Fig. 15 shows a picture of the actual displacement of the moving platform when y=1mm, the experimental results show that the actual displacement is 1.003296mm, the error is 3.296μm. Fig. 16 shows a picture of the actual displacement of the moving platform when y=6mm, the experimental results show that the actual displacement is 6.010391mm, the error is 10.391μm.

The experimental results show that the actual displacements based on elastokinematic analysis are very close to the desired displacements. A more precise positioning can be achieved based on above elastokinematic model.

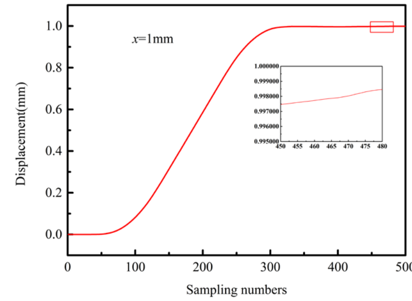

Fig. 13. The actual displacements of the moving platform when x=1mm.

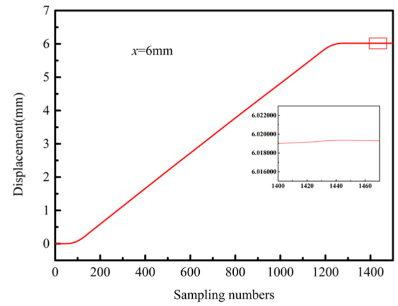

Fig. 14. The actual displacements of the moving platform when x=6mm.

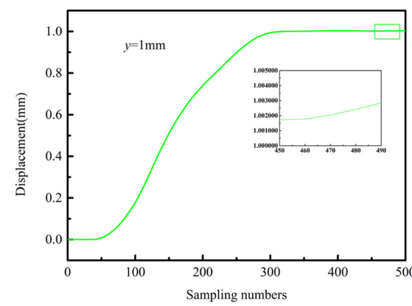

Fig. 15. The actual displacements of the moving platform when y=1mm.

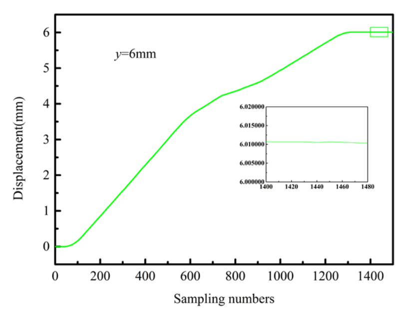

Fig. 16. The actual displacements of the moving platform when y=6mm.

VI. Conclusion

In this paper, we present an elastokinematic analysis based inverse kinematics solution of a 6-PSS compliant parallel platform for optoelectronic packaging. The elastokinematic model considers the elastic deformation and the displacement of the rotation center in the large-stroke flexure hinges. The simulation results show that the forward and the inverse kinematics solutions obtained by the elastokinematic model have very small errors compared with FEA model. The experimental results show that the actual displacements based on elastokinematic analysis are very close to the desired displacements. It can be concluded that the elastokinematic analysis is efficient for modeling the compliant parallel platforms with large-stroke flexure hinges.

REFERENCES

[1] T. Mizumoto, Y. Shoji, "Recent progress in optical nonreciprocal devices for silicon photonics," *2015 IEEE Photonics Conference (IPC)*, 2015, pp. 398-399.

[2] S. H. Jeong, G. H. Kim and K. R. Cha, "A study on optical device alignment system using ultra precision multi-axis stage," *Journal of Materials Processing Technology*, vol. 187, no. 3, pp. 65-68, 2007.

[3] L. Liang, Y. N. Zhang, L. Y. Shen and J. W. Qian, "Design and Analysis of a Parallel Robot with Flexure Hinges for Target Alignment System," *Applied Mechanics & Materials*, vol. 303-306, pp. 1647-1652, 2013.

[4] Z. J. Du, R. C. Shi and W. Dong, "A Piezo-Actuated High-Precision Flexible Parallel Pointing Mechanism: Conceptual Design, Development, and Experiments," *IEEE Transactions on Robotics*, vol. 30, no. 1, pp. 131-137, 2017.

[5] D. Kang and D. Gweon, "Development of flexure based 6-degrees of freedom parallel nano-positioning system with large displacement," *Review of Scientific Instruments*, vol. 83, no. 3, pp. 035003, 2012.

[6] W. Dong, Z. J. Du and L. N. Sun, "Stiffness influence atlases of a novel flexure hinge-based parallel mechanism with large workspace," *2005 IEEE/RSJ International Conference on Intelligent Robots and Systems*, Edmonton. Alta. Canada, 2005, pp. 856-861.

[7] Y. Yun and Y. M. Li, "Design and analysis of a novel 6-DOF redundant actuated parallel robot with compliant hinges for high precision positioning," *Nonlinear Dynamics*, vol. 61, no. 4, pp. 829-845, 2010.

[8] O. A. Turkkan and H. J. Su, "A general and efficient multiple segment method for kinetostatic analysis of planar compliant mechanisms," *Mechanism & Machine Theory*, vol. 112, pp. 205-217, 2017.

[9] A. Midha, L. L. Howell and T. W. Norton, "Limit positions of compliant mechanisms using the pseudo-rigid-body model concept," *Mechanism & Machine Theory*, vol. 35, no. 1, pp. 99-115, 2000.

[10] S. G. Bapat, "On the design and analysis of compliant mechanisms using the pseudo-rigid-body model concept," *Dissertations & Theses-Gradworks*, 2015.

[11] Y. Tian, B. Shirinzadeh and D. Zhang, "Closed-form compliance equations of filleted V-shaped flexure hinges for compliant mechanism design," *Precision Engineering*, vol. 34, no. 3, pp. 408-418, 2010.

[12] M. Liu, X. M. Zhang and S. Fatikow, "Design and analysis of a multi-notched flexure hinge for compliant mechanisms," *Precision Engineering*, vol. 48, pp. 292-304, 2017.

[13] D. Wang and R. Fan, "Design and nonlinear analysis of a 6-DOF compliant parallel manipulator with spatial beam flexure hinges," *Precision Engineering*, vol. 45, pp. 365-373, 2016.

[14] H. Shi, H. J. Su, N. Dagalakis and J. A. Kramar, "Kinematic modeling and calibration of a flexure based hexapod nanopositioner," *Precision Engineering*, vol. 37, no. 1, pp. 117-128, 2013.

[15] E. Rouhani and M. J. Nategh, "An elastokinematic solution to the inverse kinematics of microhexapod manipulator with flexure joints of varying rotation center," *Mechanism & Machine Theory*, vol. 97, pp. 127-140, 2016.

[16] Y. Koseki, T. Tanikawa, N. Koyachi and T. Ara, "Kinematic analysis of translational 3-DOF micro parallel mechanism using matrix method," *2000 IEEE/RSJ International Conference on Intelligent Robots and Systems (IROS 2000)*, Takamatsu. Japan, 2000, pp. 786-792.

[17] Q. S. Xu and Y. M. Li, "Stiffness Modeling of a Spatial 3-DOF Compliant Parallel Micromanipulator," *2006 IEEE/RSJ International Conference on Intelligent Robots and Systems*, Beijing. China, 2006, pp. 300-305.

Fulong Hou was born in Shanxi, China, in 1994. He received the B.E. degree from the College of Mechanical Engineering, Taiyuan University of Science and Technology, Taiyuan, China, in 2016. He is currently working toward the M.E. degree in mechanical engineering from Central South University, Changsha, China. His research direction is compliant parallel platforms.

Meizhu Luo received the B.E. degree from the Harbin Institute of Technology (HIT), Harbin, China, in 2011 and has been received the M.E. degree at Central South University, Changsha, China, in 2018. He researches on motor drive system, high-Precision motion platform.

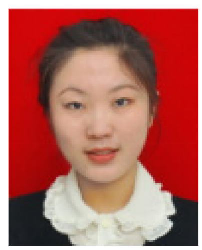

Zijiao Zhang received the B.E. and M.E. degrees from Harbin Institute of Technology (HIT), Harbin, China, in 2011 and 2013, respectively. She received the Ph.D. degree from Central South University, Changsha, China, in 2017. She is an Assistant Professor in the College of Electrical and Information Engineering, Hunan University. Her research areas are permanent magnet linear synchronous motors and linear electromagnetic propulsion.